

Replay-Free Continual Low-Rank Adaptation with Dynamic Memory

Huancheng Chen^{1,2}, Jingtao Li¹, Weiming Zhuang¹, Chen Chen¹, Lingjuan Lyu^{1,*}

¹Sony AI, ²University of Texas at Austin

huanchengch@utexas.edu, {jingtao.li, weiming.zhuang, ChenA.Chen, lingjuan.lyu}@sony.com

Abstract

We revisit continual learning (CL), which enables pre-trained vision transformers (ViTs) to sequentially fine-tune on new downstream tasks over time. However, as the scale of these models increases, catastrophic forgetting remains a more serious challenge. Recent studies highlight a crossover between CL techniques and parameter-efficient fine-tuning (PEFT), which focuses on fine-tuning only a small set of trainable parameters to adapt to downstream tasks, such as low-rank adaptation (LoRA). Several LoRA-based CL methods have been proposed to avoid forgetting by decoupling representations learned from previous tasks and those learned for new tasks, achieving a fixed balance between stability and plasticity, yet lacking mechanisms to dynamically adjust learned representations over time. To address this gap, we propose a novel PEFT-CL method called Dual Low-Rank Adaptation (DualLoRA), which introduces both an orthogonal LoRA adapter and a residual LoRA adapter parallel to pre-trained weights in each layer. These components are orchestrated by a dynamic memory mechanism to strike a balance between stability and plasticity. Additionally, we propose a scheme to predict task identity with confidence and calibrate the model’s outputs accordingly. On ViT-based models, we demonstrate that DualLoRA offers significant advantages in accuracy, inference speed, and computation efficiency in training over existing CL methods across multiple benchmarks.

1. Introduction

Continual learning (CL) [25], which aims to train models on a sequence of tasks, often suffers from *catastrophic forgetting*—a substantial degradation in performance on previously learned tasks when adapting to new ones. This challenge persists even when continually fine-tuning vision foundation models [28, 29], despite their strong generalization capability and robustness. Replay-based CL methods [1] attempt to alleviate forgetting by retaining a subset

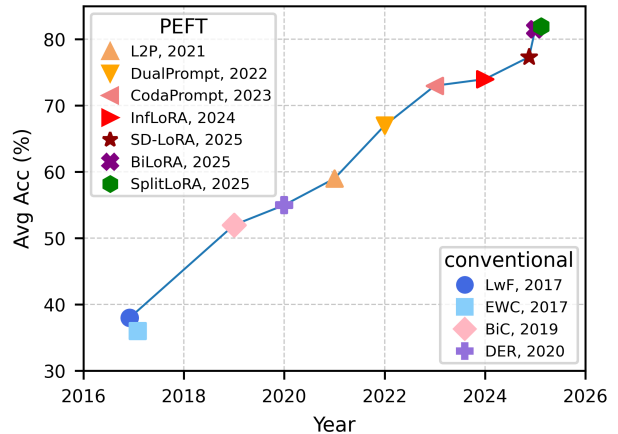


Figure 1. PEFT-based continual learning schemes dominate the ImageNet-R dataset in recent years.

of data from prior tasks as *exemplars*; however, such approaches are often impractical due to storage constraints and data retention policies. Alternatively, architecture-based CL methods [16] mitigate interference by allocating task-specific parameters and relying on task identifiers during training. Nevertheless, modifying the architecture of vision foundation models for downstream adaptation may undermine their pre-trained representations, as these weights are learned under a fixed architectural design. Moreover, many of these methods assume access to task identity at inference time—an assumption that is frequently violated in real-world scenarios.

Recently, parameter-efficient fine-tuning (PEFT) techniques have attracted increasing attention for their ability to adapt foundation models to downstream tasks by updating or introducing only a small number of trainable parameters. Beyond computational efficiency, PEFT methods have also demonstrated notable robustness in mitigating catastrophic forgetting under sequential task adaptation. In particular, prompt-tuning [24, 28, 29] and low-rank adaptation (LoRA) [14] have emerged as two widely adopted PEFT paradigms, achieving strong performance in contin-

*Corresponding Author: Lingjuan Lyu

ual learning and substantially outperforming conventional CL approaches on established benchmarks. Prompt-tuning methods learn a *prompt pool* that matches an input image with a set of prompt vectors to align image features with patch tokens. However, existing prompt-based CL approaches rely on the original pre-trained encoder as the query function. Consequently, image tokens must be processed through the backbone network **twice**, resulting in considerable computational overhead and increased inference latency.

In contrast, LoRA-based methods typically require fewer trainable parameters to achieve comparable performance on domain-specific tasks and enable faster inference than prompt-tuning. Nevertheless, vanilla LoRA [9] struggles in continual learning settings due to severe interference across sequential tasks. Inspired by gradient projection techniques [23], InfLoRA [14] takes an initial step toward addressing this issue by initializing LoRA adapters for new tasks within a subspace orthogonal to the gradient subspace of previously learned tasks. Building upon this idea, a series of follow-up studies [7, 18, 21, 30, 33] move beyond the strict orthogonality constraint imposed by InfLoRA and explore diverse forms of separated learning spaces, such as almost-orthogonal subspaces, principal-residual subspaces, and shared-specific subspaces, to better balance the stability-plasticity trade-off in continual learning. However, these LoRA-based CL methods still rely on a fixed set of adapted model weights during inference and do not incorporate dynamic adaptation of learned representations, which could further mitigate catastrophic forgetting.

To address this limitation, we propose a novel continual learning framework termed dual low-rank adaptation (DualLoRA). DualLoRA integrates an orthogonal adapter and a residual adapter into each layer of pre-trained vision transformers (ViTs). Specifically, the orthogonal adapter \mathbf{O} is updated exclusively along directions orthogonal to the feature subspaces extracted from previously learned tasks, while the residual adapter \mathbf{R} is updated within a task-specific subspace spanned by residual bases derived from prior tasks. This design promotes *stability*—by preventing interference with previously acquired knowledge through orthogonal adapters—while simultaneously enhancing *plasticity* via residual adapters that facilitate efficient adaptation to new tasks.

DualLoRA efficiently extracts orthogonal bases from the feature subspaces of past tasks and projects the updates of \mathbf{O} and \mathbf{R} using matrices constructed from these bases. Moreover, these bases are further leveraged at inference time to dynamically modulate the residual adapters based on input-specific task relevance, thereby suppressing components that may degrade test performance. We refer to this inference-time mechanism as *dynamic memory* (DM), as illustrated in Fig. 2. Extensive experimental re-

sults demonstrate that DualLoRA consistently outperforms existing PEFT-based continual learning methods across diverse benchmarks, without incurring significant additional computational or memory overhead. The main contributions of this paper are summarized as follows:

- We introduce a novel low-rank adaptation paradigm for fine-tuning ViTs in continual learning settings. This paradigm efficiently extracts feature subspaces from previously learned tasks using singular value decomposition and mitigates catastrophic forgetting by reducing task interference through gradient projection.
- To address the challenge of limited update space due to gradient projection, we design a dual LoRA structure consisting of an orthogonal adapter and a residual adapter. This design incorporates the proposed dynamic memory mechanism, effectively balancing stability and plasticity in continual learning.
- To further enhance the performance of DualLoRA, we develop a simple and efficient method for inferring task identities of test samples during inference, leveraging the extracted feature subspaces. Extensive experimental results demonstrate the superior performance of DualLoRA compared to state-of-the-art baselines.

2. Background and Related Work

2.1. Gradient Projection in CL

Gradient projection is widely employed in continual learning to mitigate catastrophic forgetting by updating parameters in directions that minimize interference with previously learned tasks. OGD [4] was the first to implement gradient descent in directions orthogonal to the stored gradient directions computed from previous tasks. The follow-up work GPM [23] extracts orthogonal bases of task representations from randomly selected training data via singular value decomposition (SVD). A subsequent study, TRGP [15], introduces the concept of a trust region, allowing partial reuse of selected bases from previous tasks. FSDGPM [3] further evaluates the importance of bases in GPM by assessing the sharpness of the loss landscape, assigning weights to the bases in the projection matrix according to their relative importance. Due to the computational expense of determining loss landscape sharpness, SGP [22] offers an alternative by using accumulated singular values as an importance indicator to scale the projection matrix in GPM. Additionally, several studies [2, 11, 13, 26, 31] have explored relaxing the orthogonality constraints and optimizing the relaxation factor to enhance performance. However, these approaches are primarily developed for relatively simple models such as CNNs and face significant challenges when applied to advanced architectures like ViTs. For instance, the high dimensionality of feature embeddings in ViTs leads to substantial computational overhead when performing SVD.

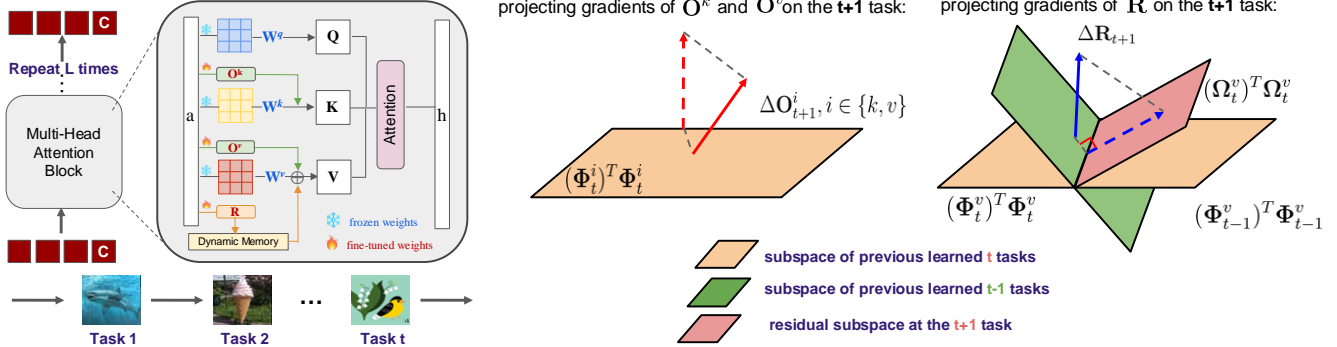


Figure 2. Illustration of our proposed DualLoRA paradigm (left) and design insights of orthogonal adapter and residual adapter (right), where the solid arrow denotes the original update and the dashed arrow denotes the projected update.

This motivates us to explore more efficient methods for extracting orthogonal bases from feature subspaces in ViTs.

2.2. Parameter-Efficient Fine-Tuning in CL

Parameter-efficient fine-tuning (PEFT) methods adapt pre-trained models to downstream tasks by fine-tuning only a small number of parameters. Among them, prompt-tuning [12] has shown strong robustness in sequential learning and achieved remarkable success in continual learning benchmarks, significantly outperforming traditional continual learning schemes. The pioneering work L2P [29] addresses continual learning by introducing a prompt pool that selects the top- k relevant queries as supplementary inputs to facilitate feature alignment in the pre-trained model. DualPrompt [28] further introduces task-invariant *G-Prompts* and task-specific *E-Prompts* to capture both shared and task-specific knowledge across tasks. S-Prompt [27] learns domain-specific prompts by applying K-means clustering to training features and using a K-NN algorithm to match test samples with corresponding prompts. CodaPrompt [24] shifts from fixed instance-specific prompts to a set of prompt components, selecting a weighted combination for each sample. Moreover, several studies [6, 19, 32] propose fine-tuning expandable prompt adapters to improve model learnability. Despite their success, these methods require forwarding training and testing samples through a query function (typically the original pre-trained model) to extract features before fine-tuning and inference, resulting in longer training and inference times.

Recently, PGP [20] and VPT-NSP [17] adapt the idea of GPM [23] to prompt-tuning by applying orthogonal projection to prompt gradients to mitigate forgetting, but inherit the drawbacks of prompt-tuning. Similarly, InfLoRA [14] is the first to apply gradient projection to low-rank adaptation for ViT models by storing gradient directions from learned tasks during fine-tuning. Several follow-up studies further extend LoRA-based continual learning. CL-LoRA [7]

decomposes LoRA parameters into task-shared and task-specific components to balance stability and plasticity. SD-LoRA [30] introduces a scalable decoupled LoRA design to better separate task knowledge. Split-LoRA [21] splits the gradient space into complementary subspaces to improve stability-plasticity trade-offs. BiLoRA [33] enforces almost-orthogonal parameter spaces across tasks to reduce interference. KeepLoRA [18] adapts LoRA updates via residual gradient modulation to preserve previously learned knowledge.

3. Preliminary

3.1. Continual Learning Problem Setting

Given a pre-trained model with backbone parameters \mathbf{W}_0 , we aim to fine-tune the model by adding adapters \mathcal{A}_l in the l -th layer of the model and the classifier \mathcal{F} to fit a sequence of domain data $\mathcal{D}_t = \{\mathbf{x}_i, \mathbf{y}_i\}_{i=1}^{|\mathcal{D}_t|}$, where \mathbf{x}_i denotes data samples and $\mathbf{y}_i \in \mathcal{Y}_t$ denotes corresponding labels in the t -th task. In the challenging class-incremental setting, there is no intersection between the label sets from two different tasks as $\mathcal{Y}_{t_1} \cap \mathcal{Y}_{t_2} = \emptyset$ for all $t_1 \neq t_2$. When learning a new task, access to old task data might become unavailable due to storage constraints. The objective function in continual learning is to minimize the empirical risk of the unified adapters $\mathcal{A}_{1:L}$ integrated in L layers of the pre-trained model that performs inference on the sequence of data from T various tasks as follows:

$$\min_{\{\mathcal{A}_l\}_{l=1, \mathcal{F}}} \frac{1}{T} \sum_{t=1}^T \mathcal{L}_{\text{task}}(\mathbf{W}_0, \mathcal{A}_{1:L}, \mathcal{F}, \mathcal{D}_t), \quad (1)$$

where \mathbf{W}_0 is the frozen backbone parameters of the pre-trained model; $\mathcal{L}_{\text{task}}(\cdot)$ is the loss function depending on the specific task. The classifier \mathcal{F} consists of an expanding set of fully-connected layers $f_t : \mathbb{R}^d \rightarrow \mathbb{R}^{C_t}$, where d is the dimension of embedding and C_t is the number of classes in

the t -th task. Given **no task identities** during inference, all the learned $f_t(\cdot)$ are used to predict categories of input data.

3.2. Multi-Head Attention Block

Vision transformer (ViT) models break down images into n patches and flatten these patches into patch embeddings of dimension d . The encoder of a ViT consists of a sequence of multi-head attention (MHA) blocks containing *key*, *query* and *value* weights \mathbf{W}^q , \mathbf{W}^k and \mathbf{W}^v for mapping input activation signals $\mathbf{a}^{(l)}$ into $\mathbf{Q}^{(l)}$, $\mathbf{K}^{(l)}$ and $\mathbf{V}^{(l)}$ and obtaining the output signals $\mathbf{h}^{(l)}$ by computing

$$\mathbf{h}^{(l)} = \text{softmax} \left(\frac{\mathbf{Q}^{(l)} (\mathbf{K}^{(l)})^\top}{\sqrt{d}} \right) \cdot \mathbf{V}^{(l)}, \quad (2)$$

where $\mathbf{Q}^{(l)} := \mathbf{a}^{(l)} \mathbf{W}^q$, $\mathbf{K}^{(l)} := \mathbf{a}^{(l)} \mathbf{W}^k$ and $\mathbf{V}^{(l)} := \mathbf{a}^{(l)} \mathbf{W}^v$. The output signals $\mathbf{h}^{(l)}$ are input to the feed-forward network and passed through normalization before being forwarded to the next MHA block until $\mathbf{h}^{(L)}$ is directed to the classifier.

3.3. Low-Rank Adaptation

Low-rank adaptation (LoRA) is a parameter-efficient fine-tuning method that enables reducing memory consumption by assigning learnable low-rank matrices $\mathbf{A} \in \mathbb{R}^{r \times d}$ and $\mathbf{B} \in \mathbb{R}^{d \times r}$ parallel to the frozen pre-trained weights $\mathbf{W}_0 \in \mathbb{R}^{d \times d}$ into each layer of the model as follows,

$$\mathbf{W} := \mathbf{W}_0 + \mathbf{B}\mathbf{A}, \quad (3)$$

where \mathbf{W} denotes model weights after fine-tuning, and $r \ll d$. In this paper, we follow the strategy in [5], and only implement LoRA fine-tuning on \mathbf{W}_0^k and \mathbf{W}_0^v while keeping \mathbf{W}_0^q frozen during the whole procedure.

4. Methodology: Dual Low-Rank Adaptation

The subspace for updating the model becomes more constrained as the gradients are projected into a subspace orthogonal to all feature subspaces from the previous tasks. Subsequent studies [3, 15, 26, 31] ease the stringent constraints of orthogonality to expand the optimization subspace in a new task, considering the stability-plasticity trade-off. Inspired by the prior studies, we propose a novel low-rank adaptation structure, DualLoRA, consisting of an orthogonal adapter $\mathbf{O} := \mathbf{A}_o \mathbf{B}_o \in \mathbb{R}^{d \times d}$ and a residual adapter $\mathbf{R} := \mathbf{A}_r \mathbf{B}_r \in \mathbb{R}^{d \times d}$ that are updated in the orthogonal direction and residual direction, as shown in Fig 2. We follow the strategy in the existing PEFT continual learning schemes [14, 20, 24, 28, 29], using pre-trained vision transformers (ViTs) as backbone models throughout this paper. In the forthcoming sections, we will illustrate the process of updating both adapters and integrating dynamic memory during model inference.

4.1. Orthogonal Adapter

The milestone work GPM [23], which uses orthogonal gradient projection to mitigate forgetting, involves flattening feature maps extracted by convolutional kernels into vectors and performing singular value decomposition (SVD) on these vectors to obtain orthogonal feature bases. However, vectorizing the patch embeddings of a ViT with dimensions (n, d) necessitates extensive computation in SVD, particularly when dealing with high-resolution inputs. In vision transformers, feature embeddings are often redundant for classification tasks, as only the first embedding (commonly referred to as the *class token*) is passed to the classifier for prediction.

To this end, we propose an efficient method for extracting the orthogonal bases of the class-token subspace without performing SVD on the entire high-dimensional embedding space. Specifically, given the pre-trained weights \mathbf{W}_0^q , \mathbf{W}_0^k , and \mathbf{W}_0^v , the fine-tuned *key* and *value* weights, i.e., \mathbf{W}_{t+1}^k and \mathbf{W}_{t+1}^v , for the $(t+1)$ -th task can be derived as follows:

$$\mathbf{W}_{t+1}^k = \mathbf{W}_0^k + \sum_{\tau=1}^{t+1} \Delta \mathbf{O}_\tau^k = \mathbf{W}_t^k + \Delta \mathbf{O}_{t+1}^k, \quad (4)$$

$$\mathbf{W}_{t+1}^v = \mathbf{W}_0^v + \sum_{\tau=1}^{t+1} \Delta \mathbf{O}_\tau^v = \mathbf{W}_t^v + \Delta \mathbf{O}_{t+1}^v, \quad (5)$$

where $\Delta \mathbf{O}_\tau^k, \Delta \mathbf{O}_\tau^v$ are the updates of the orthogonal adapter computed from the τ -th task. According to (2), when we fine-tune the parameters on the $(t+1)$ -th task, the change of output signal $\mathbf{h}^{(l)}$ given the same data can be formulated as

$$\begin{aligned} \Delta \mathbf{h}^{(l)} \approx & \Gamma \cdot \frac{\mathbf{Q}^{(l)} (\mathbf{a}^{(l)} \Delta \mathbf{O}_{t+1}^k)^\top}{\sqrt{d}} \cdot \mathbf{V}^{(l)} \\ & + \underbrace{\text{softmax} \left(\frac{\mathbf{Q}^{(l)} (\mathbf{K}^{(l)})^\top}{\sqrt{d}} \right)}_{\mathbf{S}^{(l)}} \cdot \mathbf{a}^{(l)} \Delta \mathbf{O}_{t+1}^v, \end{aligned} \quad (6)$$

where Γ is a diagonal matrix (the derivation is deferred to Appendix A.1). To preserve the value of the class token in $\mathbf{h}^{(L)}$ output by the last layer, we must restrict the value of $\Delta \mathbf{h}_1^{(l)} \approx \mathbf{0}$ (the change of the first row in $\mathbf{h}^{(l)}$) for each layer so that the class token of the same test sample from old tasks can be preserved after fine-tuning on the new task. Since $\mathbf{Q}^{(l)}$ is unchanged with the frozen weight \mathbf{W}_0^q , we need to project $\Delta \mathbf{O}_{t+1}^k$ into the subspace orthogonal to the subspace spanned by $\mathbf{k}^{(l)} := \mathbf{Q}_1^{(l)}$, denoting the first row of $\mathbf{Q}^{(l)}$. Meanwhile, $\Delta \mathbf{O}_{t+1}^v$ must be orthogonal to the subspace of $\mathbf{v}^{(l)} := \mathbf{S}_1^{(l)}$, the first row of $\mathbf{S}^{(l)}$. Following the strategy in GPM [23], we randomly sample m data points from the current task after fine-tuning on the t -th task and input these

m samples to the model for obtaining embedding matrices $\tilde{\mathbf{K}}^{(l)} \in \mathbb{R}^{m \times d}$ consisting of $\{\mathbf{k}_i^{(l)}\}_{i=1}^m$ and $\tilde{\mathbf{V}}^{(l)} \in \mathbb{R}^{m \times d}$ consisting of $\{\mathbf{v}_i^{(l)}\}_{i=1}^m$. We update the new feature matrices Φ_t^k and Φ_t^v by extracting the orthogonal bases of $\tilde{\mathbf{K}}^{(l)}$ and $\tilde{\mathbf{V}}^{(l)}$ using SVD and concatenating them into the previous feature matrices Φ_{t-1}^k and Φ_{t-1}^v . With the feature matrices obtained on the t -th task, we can project the updates $\Delta \mathbf{O}_{t+1}^k$ and $\Delta \mathbf{O}_{t+1}^v$ by

$$\Delta \mathbf{O}_{t+1}^i \leftarrow \Delta \mathbf{O}_{t+1}^i - (\Phi_t^i)^\top \Phi_t^i \Delta \mathbf{O}_{t+1}^i, \quad \forall i \in \{k, v\}. \quad (7)$$

When we select m data points, with $m \ll d$, for extracting orthogonal bases, the complexity of SVD is $\mathcal{O}(m^2 d)$, which is much more efficient than SVD with $\mathcal{O}(d^3)$ implemented in the previous work InfLoRA [14]. We emphasize that our orthogonal adapters undergo a different update process than InfLoRA, where orthogonal bases are extracted from the gradient subspace. Instead, we develop an alternative feature set, $\mathbf{S}^{(l)}$, specifically to preserve the class token, as outlined in (6). Since we only extract the orthogonal subspace from $\Delta \mathbf{h}_1^{(l)}$, we cannot guarantee that $\Delta \mathbf{h}_1^{(l)} = \mathbf{0}$ in every layer. However, reducing the magnitude of $\Delta \mathbf{h}_1^{(l)}$ can mitigate catastrophic forgetting, even if the value is not zero (details are provided in Appendix A.2).

4.2. Residual Adapter

As the feature subspaces represented by Φ_t^k and Φ_t^v expand with the accumulation of learned tasks, the majority of the components in the updates, $\Delta \mathbf{O}_{t+1}^k$ and $\Delta \mathbf{O}_{t+1}^v$, are progressively subtracted, as detailed in (7). Consequently, the update magnitudes approach zero, resulting in diminished performance during fine-tuning on new tasks. To address this issue, we introduce a residual adapter \mathbf{R}_{t+1} (initialized as $\mathbf{0}$) in parallel with \mathbf{O}_{t+1}^v , providing extra capacity for new tasks and maintaining a balance between stability and plasticity.

When the model is fine-tuned on the $(t+1)$ -th task, the residual adapter \mathbf{R}_{t+1} is updated within the subspace \mathcal{R}_t spanned by Ψ_t (we set $\Psi_1 = \emptyset$) defined as

$$\Psi_t := \Phi_t^v \setminus \Phi_{t-1}^v \subseteq \mathbb{R}^d, \quad (8)$$

where Φ_t^v and Φ_{t-1}^v are obtained after fine-tuning on the t and $t-1$ tasks. It is worth noting that the subspaces \mathcal{R}_t and \mathcal{R}_{t+1} are specific to their corresponding tasks t and $t+1$, respectively, as $\Psi_{t+1} \cap \Psi_t = \emptyset$. Specifically, the subspace \mathcal{R}_t indicates the residual knowledge extracted from the most recent task, providing supplementary bases to enlarge the optimization subspace. With these extracted bases, we are able to project the updates $\Delta \mathbf{R}_{t+1}$ into the subspace \mathcal{R}_t by

$$\Delta \mathbf{R}_{t+1} \leftarrow \Psi_t^\top \Psi_t \Delta \mathbf{R}_{t+1}. \quad (9)$$

When we conduct **fine-tuning** on the $(t+1)$ -th task, the value matrix $\mathbf{V}^{(l)}$ in the l -th layer given the input activations

$\mathbf{a}^{(l)}$ can be found as

$$\mathbf{V}^{(l)} = \mathbf{a}^{(l)} (\mathbf{W}_0^v + \mathbf{O}_{t+1}^v) + \mathbf{a}^{(l)} \mathbf{R}_{t+1} = \mathbf{V}_o^{(l)} + \mathbf{V}_r^{(l)}, \quad (10)$$

where \mathbf{W}_0^v denotes the pre-trained weights, and $\mathbf{V}_o^{(l)} := \mathbf{a}^{(l)} (\mathbf{W}_0^v + \mathbf{O}_{t+1}^v)$, $\mathbf{V}_r^{(l)} := \mathbf{a}^{(l)} \mathbf{R}_{t+1}$.

4.3. Dynamic Memory

As previously mentioned, the residual adapter \mathbf{R}_{t+1} is updated within the subspace \mathcal{R}_t , a subset of the feature subspace spanned by Φ_t extracted from the t -th task. Consequently, the fine-tuning process may deteriorate the performance on prior tasks. To mitigate this issue, we introduce a *dynamic memory* mechanism that adjusts the value of $\mathbf{V}_r^{(l)}$, which is the output of \mathbf{R}_{t+1} during **inference** on test data according to

$$\hat{\mathbf{V}}^{(l)} = \mathbf{V}_o^{(l)} + \mathbf{a}^{(l)} \Omega_{t+1}^\top \Omega_{t+1} \mathbf{R}_{t+1} = \mathbf{V}_o^{(l)} + \hat{\mathbf{V}}_r^{(l)}, \quad (11)$$

where $\Omega_{t+1}^\top \Omega_{t+1}$ is computed according to the input activation signal $\mathbf{a}^{(l)}$. Specifically, the attention score $\mathbf{S}^{(l)} \propto \text{softmax}\left(\frac{\mathbf{Q}^{(l)} (\mathbf{K}^{(l)})^\top}{\sqrt{d}}\right)$, computed by applying $\mathbf{a}^{(l)}$ to the query and key weight matrices, reflects the relevance between the input test sample and the task associated with the extracted bases used to update the residual adapter \mathbf{R}_{t+1} . We utilize the matrices $\Psi_\tau \in \mathbb{R}^{r_\tau \times d}$ ($\tau \leq t+1$), stored in memory, to multiply the first row of the attention score, $\mathbf{v}^{(l)} := \mathbf{S}_1^{(l)}$, as follows:

$$\text{if } r_\tau \neq 0, \omega_\tau = \frac{\|\Psi_\tau \mathbf{v}^{(l)}\|}{r_\tau \|\mathbf{v}^{(l)}\|}, \quad \text{otherwise, } \omega_\tau = 0, \quad (12)$$

where r_τ indicates the rank of Ψ_τ . Since the task-specific residual bases remain independent across different tasks, the cosine similarity between feature vectors $\mathbf{v}^{(l)}$ extracted from input test samples and the stored residual bases Ψ_τ for each task can be used as a scaling factor for the corresponding components in the outputs of the residual adapter. This method assigns lower weights to components irrelevant to the current test samples, while components with high relevance to the samples are given proportionally higher weights. The resulting matrix Ω_{t+1} is obtained by

$$\Omega_{t+1} = \begin{bmatrix} \Sigma_1 & \mathbf{0} & \cdots & \mathbf{0} \\ \mathbf{0} & \Sigma_2 & \cdots & \mathbf{0} \\ \vdots & & \ddots & \vdots \\ \mathbf{0} & \mathbf{0} & \cdots & \Sigma_{t+1} \end{bmatrix} \begin{bmatrix} \Psi_1 \\ \Psi_2 \\ \vdots \\ \Psi_{t+1} \end{bmatrix} \in \mathbb{R}^{r' \times d}, \quad (13)$$

where $r' = \sum_{\tau=1}^{t+1} r_\tau$ and $\Sigma_\tau \in \mathbb{R}^{r_\tau \times r_\tau}$ is a diagonal matrix with identical entries $\omega_\tau^{1/2}$.

4.4. Task Identification with Confidence

As the number of fully connected layers $f_t(\cdot)$ increases with the addition of tasks during continual learning, there is a

Table 1. Metrics (%) computed from experiments on ImageNet-R. We report the average accuracy over 3 trials, each with different random seeds. The numeric after "±" denotes standard deviation.

Method	5-Split ImageNet-R		10-Split ImageNet-R		20-Split ImageNet-R	
	ACC(↑)	FT(↓)	ACC(↑)	FT(↓)	ACC(↑)	FT(↓)
LoRA	72.33 ±0.94	12.1 ±1.19	61.85 ±0.52	26.0 ±1.35	48.59 ±0.39	34.4 ±0.57
L2P	61.60 ±0.43	5.36 ±0.27	59.21 ±0.68	7.59 ±0.78	56.36 ±0.83	10.3 ±0.72
DualPrompt	68.47 ±0.23	3.18 ±0.24	66.72 ±0.30	4.15 ±0.11	64.40 ±0.18	5.82 ±0.51
PGP	69.07 ±0.28	3.41 ±0.18	64.22 ±4.53	4.23 ±0.22	64.19 ±0.38	6.50 ±0.31
S-Prompt	51.33 ±0.22	27.6 ±1.18	49.80 ±0.16	29.2 ±0.93	55.64 ±0.53	22.3 ±1.85
CodaPrompt	74.91 ±0.30	1.85 ±0.07	73.83 ±0.29	2.56 ±0.31	68.96 ±0.46	3.25 ±0.40
InfLoRA	77.30 ±0.49	3.05 ±0.44	74.03 ±0.30	6.18 ±0.25	69.77 ±0.31	7.98 ±0.40
DualLoRA	78.55 ±0.12	2.61 ±0.25	76.23 ±0.33	3.67 ±0.66	71.25 ±0.31	5.45 ±0.27
DualLoRA+	79.88 ±0.50	1.10 ±0.16	81.17 ±0.23	2.04 ±0.05	74.73 ±0.40	3.75 ±0.10

Table 2. Metrics (%) computed from experiments on CIFAR100 and Tiny-ImageNet. We report the average accuracy over 3 trials, each with different random seeds. The numeric after "±" denotes standard deviation.

Method	10-Split CIFAR100		10-Split TinyImageNet		20-Split TinyImageNet	
	ACC(↑)	FT(↓)	ACC(↑)	FT(↓)	ACC(↑)	FT(↓)
LoRA	73.32 ±0.38	20.4 ±0.53	67.69 ±0.49	23.7 ±0.65	48.48 ±2.36	44.4 ±2.73
L2P	83.97 ±0.18	6.41 ±0.09	81.90 ±0.42	5.39 ±0.33	81.24 ±0.21	5.86 ±0.22
DualPrompt	85.85 ±0.22	5.41 ±0.12	85.10 ±0.10	3.95 ±0.22	82.77 ±0.12	5.31 ±0.10
PGP	85.28 ±0.01	5.60 ±0.34	84.83 ±0.21	4.32 ±0.16	83.49 ±0.35	5.24 ±0.31
S-Prompt	67.03 ±0.66	24.8 ±0.62	68.41 ±0.26	10.41 ±0.68	74.69 ±0.30	7.70 ±0.28
CodaPrompt	85.77 ±0.69	4.07 ±0.22	85.67 ±0.25	3.16 ±0.17	83.61 ±0.47	3.34 ±0.35
InfLoRA	85.62 ±0.74	4.34 ±0.06	81.28 ±0.40	8.62 ±0.36	75.89 ±0.38	13.8 ±0.11
DualLoRA	89.13 ±0.17	4.08 ±0.16	86.42 ±0.07	3.87 ±0.18	83.75 ±0.25	5.24 ±0.15
DualLoRA+	90.94 ±0.15	3.20 ±0.18	87.74 ±0.21	2.45 ±0.25	84.65 ±0.07	3.61 ±0.13

risk that an irrelevant fully connected layer may generate the maximal logit, resulting in incorrect predictions for input test samples. This motivates us to propose a task identity prediction scheme based on task relevance, computed using Ψ_τ as described earlier in (12).

As mentioned earlier, we sample m training data points to extract orthogonal bases after completing the t -th task. During this process, we obtain the average feature vector $\bar{\mathbf{v}}^{(L)}$ forwarded to the **final** attention block from each task and compute the similarity vector $\boldsymbol{\pi}_t = \{\omega_\tau\}_{\tau=1}^t$ based on (12). Therefore, we obtain a set $\mathbf{\Pi}_t = \{\boldsymbol{\pi}_1, \dots, \boldsymbol{\pi}_t\}$ that can be used to distinguish the task identity during inference. Specifically, let $\boldsymbol{\pi}^*$ denote the similarity vector computed from the input test sample; then we can predict the **task identity** by

$$\hat{k} = \arg \max_{\tau} g(\boldsymbol{\pi}_\tau, \boldsymbol{\pi}^*), \quad (14)$$

$$g(\boldsymbol{\pi}_\tau, \boldsymbol{\pi}^*) := \frac{\|\boldsymbol{\pi}_\tau \cdot \boldsymbol{\pi}^*\|}{\|\boldsymbol{\pi}_\tau\| \cdot \|\boldsymbol{\pi}^*\|}, \quad (15)$$

$$\hat{\delta} = \lambda \left(g(\boldsymbol{\pi}_{\hat{k}}, \boldsymbol{\pi}^*) - \max_{\tau \neq \hat{k}} g(\boldsymbol{\pi}_\tau, \boldsymbol{\pi}^*) \right), \quad (16)$$

where λ is a scaling factor, \hat{k} denotes the predicted task identity, and $\hat{\delta}$ indicates the confidence of this prediction. Moreover, we scale the output logits as

$$f_{\hat{k}}(\mathbf{h}^{(L)}) \leftarrow (1 + \hat{\delta}) \cdot f_{\hat{k}}(\mathbf{h}^{(L)}). \quad (17)$$

5. Experiments

5.1. Experimental Settings

Datasets and Metrics. We evaluate the proposed method DualLoRA on three continual learning benchmark datasets: CIFAR100, Tiny-ImageNet and ImageNet-R[8]. To generate a sequence of tasks in a class-incremental setting as illustrated in (1), we randomly split the original dataset by class ID. This process creates multiple partitions, each containing an equal number of classes. Each partition corresponds to a distinct task. Following the strategy in existing studies in continual learning [20, 24, 28], we compute the final average accuracy (denoted by ACC) and degree of forgetting (denoted by FT) for evaluating the performance of

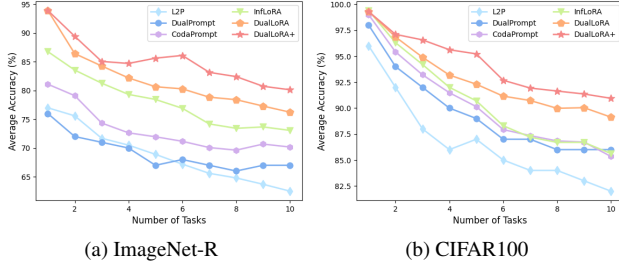


Figure 3. Figures (a) and (b) demonstrate the average accuracy of different methods during training.

our method, and these two metrics can be found as

$$\text{ACC} = \frac{1}{T} \sum_{\tau=1}^T \text{acc}_{\tau,T}, \quad (18)$$

$$\text{FT} = \frac{1}{T-1} \sum_{\tau=1}^{T-1} \text{acc}_{\tau,\text{best}} - \text{acc}_{\tau,T}, \quad (19)$$

where $\text{acc}_{\tau,T}$ denotes the accuracy of the τ -th task after the model learns the T -th task while $\text{acc}_{\tau,\text{best}}$ denotes the highest accuracy on the τ -th task during the whole fine-tuning process. Throughout the evaluation, we assume that the task identities of the testing data are **unknown**.

Baselines. Our baselines include vanilla LoRA, L2P [29], DualPrompt [28], PGP [20], S-Prompt [27], CodaPrompt [24], and InfLoRA [14]. We focus on comparing the proposed DualLoRA with the state-of-the-art PEFT-based CL schemes since they are superior to traditional CL schemes. To demonstrate the **upper-bound** performance of DualLoRA, we implemented it under the setting where all samples in a batch share the same task identity, referred to as **DualLoRA+**. In this scenario, we use average feature to compute similarity in the task identity prediction as described in Section 4.4 and facilitate more accurate task prediction, as the average feature exhibits less variance and is closer to the true mean.

Model Architecture and Hyperparameters. We use ViT-B/16 backbone pretrained on ImageNet-21K as the foundation model throughout all experiments. We use the Adam optimizer with parameters $\beta_1 = 0.9$ and $\beta_2 = 0.999$ for model fine-tuning in 5 epochs and the batchsize is set to 16 in all experiments. More details of hyperparameters are provided in Appendix B.1.

5.2. Experimental Results

ImageNet-R. As shown in Table 1, DualLoRA demonstrates comparable performance with InfLoRA, which outperforms other Prompt-based CL schemes in final

average accuracy ACC. DualLoRA exhibits a slight performance decrease compared to InfLoRA by 1.25% on the 5-split benchmark, yet it outperforms InfLoRA by 2.2% and 1.48% on the 10-split and 20-split benchmarks, respectively. Forgetting serves as another metric to quantify the performance degradation on previous tasks, which may not consistently align with the average accuracy. CodaPrompt shows superior performance in mitigating forgetting, even though it does not achieve the same level as InfLoRA and DualLoRA in the average accuracy metric. DualLoRA+ significantly enhances both average accuracy and forgetting metrics, surpassing all other baselines except for securing the second position in the forgetting metric on the 20-split benchmark. DualLoRA+ outperforms the state-of-the-art scheme InfLoRA by 2.58%, 7.14%, and 4.96% in terms of average accuracy metric across the 5-split, 10-split, and 20-split settings. In addition, in terms of the forgetting metric, DualLoRA+ shows improvements over InfLoRA by 1.95%, 4.14%, and 3.23%, respectively, in the same settings.

CIFAR100 and Tiny-ImageNet. DualLoRA steadily shows strong performance in these two datasets, achieving the best performance in average accuracy compared to prior existing schemes on CIFAR100 and Tiny-ImageNet benchmarks while slightly underperforming CodaPrompt on Tiny-ImageNet in forgetting metrics. DualLoRA+ consistently demonstrates extraordinary performance in average accuracy, outperforming CodaPrompt (the best scheme in these baselines) by 5.17%, 2.07% and 1.04%, respectively, and also demonstrating an advantage in the forgetting metric on 10-split CIFAR100 and 10-split Tiny-ImageNet. To give more insights, we report the average accuracy computed with different numbers of learned tasks, as illustrated in Fig. 3(a) and 3(b). As shown in the figures, DualLoRA and DualLoRA+ outperform other baselines in different stages of continual learning. Furthermore, DualLoRA+ demonstrates robust resistance to forgetting as the number of learned tasks increases, suggesting the potential of DualLoRA+ fine-tuning foundational models across a wider range of tasks without significant forgetting.

5.3. Ablation Study

We perform additional experiments to confirm the effectiveness of various subroutines within the DualLoRA scheme. To be specific, we implement three variants of DualLoRA: (1) **LoRA + O** stands for only using the orthogonal adapter; (2) **LoRA + O + R** stands for running DualLoRA with orthogonal and residual adapters but performing no task identity prediction; (3) **LoRA + O + R + Task ID** assumes knowing true task identities. As illustrated in Table 3, the orthogonal adapter significantly improves the performance of LoRA while the residual adapter further enhances both

Table 3. **O** stands for orthogonal adapter, **R** stands for residual adapter, and **Task ID** stands for giving true task ID during inference.

Method	10-Split ImageNet-R		10-Split CIFAR100		10-Split TinyImageNet	
	ACC(↑)	FT(↓)	ACC(↑)	FT(↓)	ACC(↑)	FT(↓)
LoRA	61.85	26.0	73.03	20.26	67.69	23.70
LoRA + O	74.11	4.65	84.03	5.67	83.92	7.74
LoRA + O + R	74.60	4.12	86.65	3.96	85.61	4.30
DualLoRA	76.23	3.67	89.13	5.08	86.42	3.87
DualLoRA+	81.17	2.04	90.94	3.20	87.74	2.45
DualLoRA + Task ID	87.66	0.46	94.39	1.05	95.71	0.84

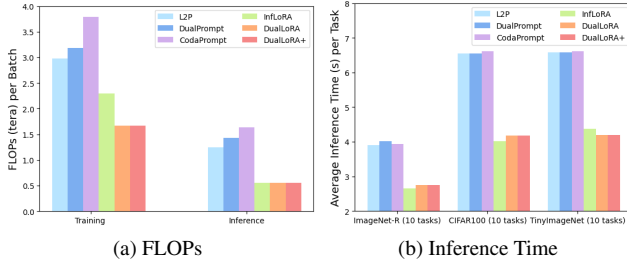


Figure 4. Figure (a) demonstrates the approximated average FLOPs during training and inference on each batch of data points. Figure (b) demonstrates the actual average running time for different schemes to perform inference on a task.

average accuracy and forgetting metrics. Moreover, DualLoRA and DualLoRA+ further improve the performance by using individual features and average features to perform task identity prediction. The final configuration, where true task identities are utilized, exhibits superior performance in both average accuracy and forgetting, highlighting the crucial role of task prediction.

5.4. Computation and Inference Time

To better compare DualLoRA with other baselines in terms of computation, we report the number of floating point operations (FLOPs) during the training and inference phases in Figure 4(a) and the average inference time on a task in Figure 4(b). According to the results in the figure, InfLoRA has the lowest FLOPs during inference, while DualLoRA has the lowest FLOPs during training because InfLoRA requires a double forward pass. During inference, InfLoRA and DualLoRA have similar inference time across different datasets, which is less than 50% inference time compared to the prompt-based CL schemes. Details on computing FLOPs are provided in Appendix B.2.

5.5. Varying the Pre-Trained Models

To evaluate the consistency of DualLoRA’s performance, we conduct experiments using the ViT-B/16 model, pre-trained on ImageNet-1k through both supervised learning and the unsupervised SAM framework [10]. To represent

Table 4. Metrics computed from experiments on ImageNet-R (10 tasks) using various pretrained ViTs beyond ImageNet-21k. **ACC** denotes the average of ACC in every timestep.

	Method	ACC(%)	$\overline{\text{ACC}}(\%)$
ImageNet-1k	L2P	60.23	67.86
	DualPrompt	67.45	72.48
	CodaPrompt	73.26	79.49
	InfLoRA	75.58	81.92
	DualLoRA	77.28	82.63
SAM-1k	L2P	52.71	58.24
	DualPrompt	56.57	63.23
	CodaPrompt	61.13	70.79
	InfLoRA	64.62	73.66
	DualLoRA	66.44	74.70

the average performance of all schemes during the continual learning process, we use $\overline{\text{ACC}} = \frac{1}{T} \sum_{t=1}^T \text{ACC}_t$ as an additional metric in the table. As shown, all schemes experience performance degradation when using a ViT model pre-trained on unsupervised datasets. Nonetheless, DualLoRA consistently outperforms other schemes in terms of average accuracy.

6. Conclusion

We introduce DualLoRA, a novel low-rank adaptation scheme for vision transformers (ViTs) that integrates orthogonal and residual adapters, operating in parallel with pre-trained weights. This structure achieves a balance between stability and plasticity in continual learning through a dynamic memory mechanism that leverages subspaces from previously learned tasks. Furthermore, we develop a task identity prediction scheme based on core bases extracted from each learned task to enhance DualLoRA’s performance. Extensive experiments demonstrate that DualLoRA outperforms state-of-the-art continual learning methods across multiple benchmarks while requiring fewer computational resources. We see this work as an important step toward developing more efficient and effective continual learning paradigms for foundational models.

References

- [1] Hyuntak Cha, Jaeho Lee, and Jinwoo Shin. Co2l: Contrastive continual learning. In *Proceedings of the IEEE/CVF International conference on computer vision*, pages 9516–9525, 2021. 1
- [2] Seohyeon Cha, Huancheng Chen, and Haris Vikalo. Task-agnostic federated continual learning via replay-free gradient projection. *arXiv preprint arXiv:2509.21606*, 2025. 2
- [3] Danruo Deng, Guangyong Chen, Jianye Hao, Qiong Wang, and Pheng-Ann Heng. Flattening sharpness for dynamic gradient projection memory benefits continual learning. *Advances in Neural Information Processing Systems*, 34: 18710–18721, 2021. 2, 4
- [4] Mehrdad Farajtabar, Navid Azizan, Alex Mott, and Ang Li. Orthogonal gradient descent for continual learning. In *International Conference on Artificial Intelligence and Statistics*, pages 3762–3773. PMLR, 2020. 2
- [5] Qiankun Gao, Chen Zhao, Yifan Sun, Teng Xi, Gang Zhang, Bernard Ghanem, and Jian Zhang. A unified continual learning framework with general parameter-efficient tuning. In *Proceedings of the IEEE/CVF International Conference on Computer Vision*, pages 11483–11493, 2023. 4
- [6] Xinyuan Gao, Songlin Dong, Yuhang He, Qiang Wang, and Yihong Gong. Beyond prompt learning: Continual adapter for efficient rehearsal-free continual learning. In *European Conference on Computer Vision*, pages 89–106. Springer, 2024. 3
- [7] Jiangpeng He, Zhihao Duan, and Fengqing Zhu. Clora: Continual low-rank adaptation for rehearsal-free class-incremental learning. In *Proceedings of the Computer Vision and Pattern Recognition Conference*, pages 30534–30544, 2025. 2, 3
- [8] Dan Hendrycks, Steven Basart, Norman Mu, Saurav Kadavath, Frank Wang, Evan Dorundo, Rahul Desai, Tyler Zhu, Samyak Parajuli, Mike Guo, et al. The many faces of robustness: A critical analysis of out-of-distribution generalization. In *Proceedings of the IEEE/CVF international conference on computer vision*, pages 8340–8349, 2021. 6
- [9] Edward J Hu, Yelong Shen, Phillip Wallis, Zeyuan Allen-Zhu, Yuanzhi Li, Shean Wang, Lu Wang, and Weizhu Chen. Lora: Low-rank adaptation of large language models. *arXiv preprint arXiv:2106.09685*, 2021. 2
- [10] Alexander Kirillov, Eric Mintun, Nikhila Ravi, Hanzi Mao, Chloe Rolland, Laura Gustafson, Tete Xiao, Spencer Whitehead, Alexander C Berg, Wan-Yen Lo, et al. Segment anything. In *Proceedings of the IEEE/CVF International Conference on Computer Vision*, pages 4015–4026, 2023. 8
- [11] Yajing Kong, Liu Liu, Zhen Wang, and Dacheng Tao. Balancing stability and plasticity through advanced null space in continual learning. In *European Conference on Computer Vision*, pages 219–236. Springer, 2022. 2
- [12] Brian Lester, Rami Al-Rfou, and Noah Constant. The power of scale for parameter-efficient prompt tuning. *arXiv preprint arXiv:2104.08691*, 2021. 3
- [13] Yan-Shuo Liang and Wu-Jun Li. Adaptive plasticity improvement for continual learning. In *Proceedings of the IEEE/CVF Conference on Computer Vision and Pattern Recognition*, pages 7816–7825, 2023. 2
- [14] Yan-Shuo Liang and Wu-Jun Li. Inflora: Interference-free low-rank adaptation for continual learning. *arXiv preprint arXiv:2404.00228*, 2024. 1, 2, 3, 4, 5, 7
- [15] Sen Lin, Li Yang, Deliang Fan, and Junshan Zhang. Trgp: Trust region gradient projection for continual learning. *arXiv preprint arXiv:2202.02931*, 2022. 2, 4
- [16] Noel Loo, Siddharth Swaroop, and Richard E Turner. Generalized variational continual learning. *arXiv preprint arXiv:2011.12328*, 2020. 1
- [17] Yue Lu, Shizhou Zhang, De Cheng, Yinghui Xing, Nannan Wang, Peng Wang, and Yanning Zhang. Visual prompt tuning in null space for continual learning. *arXiv preprint arXiv:2406.05658*, 2024. 3
- [18] Mao-Lin Luo, Zi-Hao Zhou, Yi-Lin Zhang, Yuanyu Wan, Tong Wei, and Min-Ling Zhang. Keeplora: Continual learning with residual gradient adaptation. *arXiv preprint arXiv:2601.19659*, 2026. 2, 3
- [19] Mark D McDonnell, Dong Gong, Amin Parvaneh, Ehsan Abbasnejad, and Anton Van den Hengel. Ranpac: Random projections and pre-trained models for continual learning. *Advances in Neural Information Processing Systems*, 36:12022–12053, 2023. 3
- [20] Jingyang Qiao, Xin Tan, Chengwei Chen, Yanyun Qu, Yong Peng, Yuan Xie, et al. Prompt gradient projection for continual learning. In *The Twelfth International Conference on Learning Representations*, 2023. 3, 4, 6, 7
- [21] Haomiao Qiu, Miao Zhang, Ziyue Qiao, Weili Guan, Min Zhang, and Liqiang Nie. Splitlora: Balancing stability and plasticity in continual learning through gradient space splitting. *arXiv preprint arXiv:2505.22370*, 2025. 2, 3
- [22] Gobinda Saha and Kaushik Roy. Continual learning with scaled gradient projection. In *Proceedings of the AAAI Conference on Artificial Intelligence*, pages 9677–9685, 2023. 2
- [23] Gobinda Saha, Isha Garg, and Kaushik Roy. Gradient projection memory for continual learning. *arXiv preprint arXiv:2103.09762*, 2021. 2, 3, 4
- [24] James Seale Smith, Leonid Karlinsky, Vyshnavi Gutta, Paola Cascante-Bonilla, Donghyun Kim, Assaf Arbelle, Rameswar Panda, Rogerio Feris, and Zsolt Kira. Coda-prompt: Continual decomposed attention-based prompting for rehearsal-free continual learning. In *Proceedings of the IEEE/CVF Conference on Computer Vision and Pattern Recognition*, pages 11909–11919, 2023. 1, 3, 4, 6, 7
- [25] Liyuan Wang, Xingxing Zhang, Hang Su, and Jun Zhu. A comprehensive survey of continual learning: Theory, method and application. *IEEE Transactions on Pattern Analysis and Machine Intelligence*, 2024. 1
- [26] Shipeng Wang, Xiaorong Li, Jian Sun, and Zongben Xu. Training networks in null space of feature covariance for continual learning. In *Proceedings of the IEEE/CVF conference on Computer Vision and Pattern Recognition*, pages 184–193, 2021. 2, 4
- [27] Yabin Wang, Zhiwu Huang, and Xiaopeng Hong. S-prompts learning with pre-trained transformers: An occam’s razor for domain incremental learning. *Advances in Neural Information Processing Systems*, 35:5682–5695, 2022. 3, 7

- [28] Zifeng Wang, Zizhao Zhang, Sayna Ebrahimi, Ruoxi Sun, Han Zhang, Chen-Yu Lee, Xiaoqi Ren, Guolong Su, Vincent Perot, Jennifer Dy, et al. Dualprompt: Complementary prompting for rehearsal-free continual learning. In *European Conference on Computer Vision*, pages 631–648. Springer, 2022. [1](#), [3](#), [4](#), [6](#), [7](#)
- [29] Zifeng Wang, Zizhao Zhang, Chen-Yu Lee, Han Zhang, Ruoxi Sun, Xiaoqi Ren, Guolong Su, Vincent Perot, Jennifer Dy, and Tomas Pfister. Learning to prompt for continual learning. In *Proceedings of the IEEE/CVF Conference on Computer Vision and Pattern Recognition*, pages 139–149, 2022. [1](#), [3](#), [4](#), [7](#)
- [30] Yichen Wu, Hongming Piao, Long-Kai Huang, Renzhen Wang, Wanhua Li, Hanspeter Pfister, Deyu Meng, Kede Ma, and Ying Wei. Sd-lora: Scalable decoupled low-rank adaptation for class incremental learning. *arXiv preprint arXiv:2501.13198*, 2025. [2](#), [3](#)
- [31] Zhen Zhao, Zhizhong Zhang, Xin Tan, Jun Liu, Yanyun Qu, Yuan Xie, and Lizhuang Ma. Rethinking gradient projection continual learning: Stability/plasticity feature space decoupling. In *Proceedings of the IEEE/CVF Conference on Computer Vision and Pattern Recognition*, pages 3718–3727, 2023. [2](#), [4](#)
- [32] Da-Wei Zhou, Hai-Long Sun, and et al. Expandable subspace ensemble for pre-trained model-based class-incremental learning. In *Proceedings of the IEEE/CVF Conference on Computer Vision and Pattern Recognition*, pages 23554–23564, 2024. [3](#)
- [33] Hao Zhu, Yifei Zhang, Junhao Dong, and Piotr Koniusz. Bilora: almost-orthogonal parameter spaces for continual learning. In *Proceedings of the IEEE/CVF Conference on Computer Vision and Pattern Recognition*, pages 25613–25622, 2025. [2](#), [3](#)